Articles

Discovery and Refinement of a New Structural Class of Potent Peptide Deformylase Inhibitors

Adrien Boularot,[†,‡] Carmela Giglione,[†] Sylvain Petit,[†,‡] Yann Duroc,[†] Rodolphe Alves de Sousa,[‡] Valéry Larue,[§] Thierry Cresteil,[#] Frédéric Dardel,[§] Isabelle Artaud,[‡] and Thierry Meinnel*,[†]

UPR2355 and UPR2301, Centre National de la Recherche Scientifique, Bâtiment 23, 1 Avenue de la Terrasse, F-91198 Gif-Sur-Yvette Cedex, France, and UMR8601 and UMR8015, CNRS−Université Paris V, 45 Rue des Saint-Pères and 4 Avenue de l'Observatoire, 75006 Paris, France

New classes of antibiotics are urgently needed to counter increasing levels of pathogen resistance. Peptide deformylase (PDF) was originally selected as a specific bacterial target, but a human homologue, the inhibition of which causes cell death, was recently discovered. We developed a dual-screening strategy for selecting highly effective compounds with low inhibition effect against human PDF. We selected a new scaffold in vitro that discriminated between human and bacterial PDFs. Analyses of structure−activity relationships identified potent antibiotics such as 2-(5-bromo-1*H*-indol-3-yl)-*N*-hydroxyacetamide (**6b**) with the same mode of action in vivo as previously identified PDF inhibitors but without the apoptotic effects of these inhibitors in human cells.

Introduction

Over the past decade, there has been an alarming increase in the prevalence of multiresistant phenotypes among pathogenic bacteria. There is therefore an urgent need to identify new antibiotics to combat infectious diseases. This challenge can be met by whole-cell screening or by a combination of genomics and mechanism-based drug design in cell-free assays.[1,2] The first step in this second approach is the search for vital genes unique to bacteria and conserved in various bacterial genomes. The starting criteria for suitability are essentiality and selectivity (the so-called "druggability") of the potential antibiotic target. Inhibitors of the most suitable targets are then identified by high-throughput screening in vitro, and the most promising molecules are improved by medicinal chemistry. Whole-cell studies must then be carried out on the most promising compounds, selected on the basis of optimal antibiotic capacities. Constant monitoring of the mode of action of the compound series is critical during this process.

However, a decade after its introduction, the "cell-free" approach may be considered disappointing, as it has brought to the pipeline only a couple of drugs all derived from natural products, including actinonin inhibiting peptide deformylase (PDF[a]).[3−5] The recent demonstration of the existence of a PDF homologue (mitochondrial PDF or mPDF) in humans[6−8] raised major objections to the use of this otherwise very promising target.[9,10] Indeed, mPDF proved (i) to be functional, displaying PDF activity in the human mitochondrion, (ii) to be involved in the same essential pathway as in bacteria, (iii) to be inhibited in vitro by the natural compound actinonin, used to design the compounds currently in clinical trials, and (iv) to be inhibited in vivo by actinonin in some cell lines.[6−8,11−13] Finally, when used at a range of concentrations similar to the minimal inhibitory concentrations (MIC) of the best compounds, actinonin and its derivatives had an antiproliferative effect triggered by mitochondrial dysfunction, including ATP depletion, membrane depolarization, and apoptosis induction, leading to cell death.[6,12,14,15]

Two bacterial PDF types, PDF1B and PDF2, have been distinguished.[9,16] PDF2 is found only in Gram-positive bacteria. Bacteria may have one or several functional genes encoding different types of PDF.[9,16] For example, Gram-negative *Escherichia coli* has one PDF1B gene (*def*) only, whereas Gram-positive bacteria such as *Bacillus* spp. have two PDF genes: *def*, encoding PDF1B, and *ykrB*, encoding PDF2. The human PDF (mPDF) has been classified as a PDF1A.[11]

The aim of our study was to identify new compounds that would selectively inhibit both types of bacterial PDFs (PDF1B and PDF2) without significantly inhibiting PDF1A.

Results and Discussion

Design and Medium-Throughput Screening by NMR Identify Indole Derivatives as Low-Affinity Ligands of PDF. The binding potency of peptide deformylase inhibitors (PDFI) depends essentially on the additive effects of two chemical groups: (i) a metal-binding group and (ii) the P1′ group, which binds the S1′ pocket of PDF.[4] The increase in entropy due to the binding of either of these low-affinity binding groups results in the molecule being a potent PDFI, with inhibition constants in the nanomolar range. The S1′ pocket of bacterial PDFs of both types, PDF1B and PDF2, accepts *n*-butyl, *n*-pentyl, *n*-hexyl, *n*-phenyl,[17] and other cyclic side chains[4] with low levels of selectivity. mPDF has a modified S1′ pocket that cannot tolerate bulky chains such as phenyl chains.[8,18,19] We therefore looked for bulky, cyclic compounds that would bind to bacterial PDF

* To whom correspondence should be addressed. Phone: +33 1 69 82 36 12. Fax: +33 1 69 82 36 07. E-mail: Thierry.Meinnel@isv.cnrs-gif.fr.
 † UPR2355, Centre National de la Recherche Scientifique.
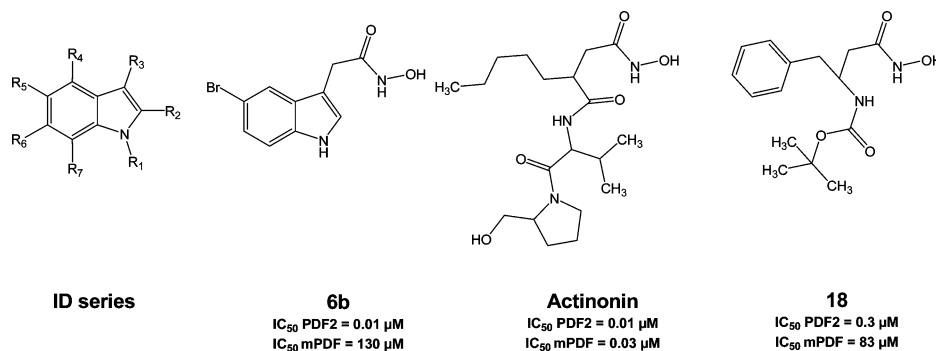 ‡ UMR8601, CNRS−Université Paris V.
 § UMR8015, CNRS−Université Paris V.
 # UPR2301, Centre National de la Recherche Scientifique.
 [a] Abbreviations: HSQC, heteronuclear single quantum correlation; IC$_{50}$, inhibition constant; ID, indole derivatives; K_I, inhibition or dissociation constant; MIC, minimum inhibitory concentration; PDF, peptide deformylase; PDFI, peptide deformylase inhibitors; SAR, structure−activity relationship; STD, saturation transfer difference; 3D, three-dimensional.
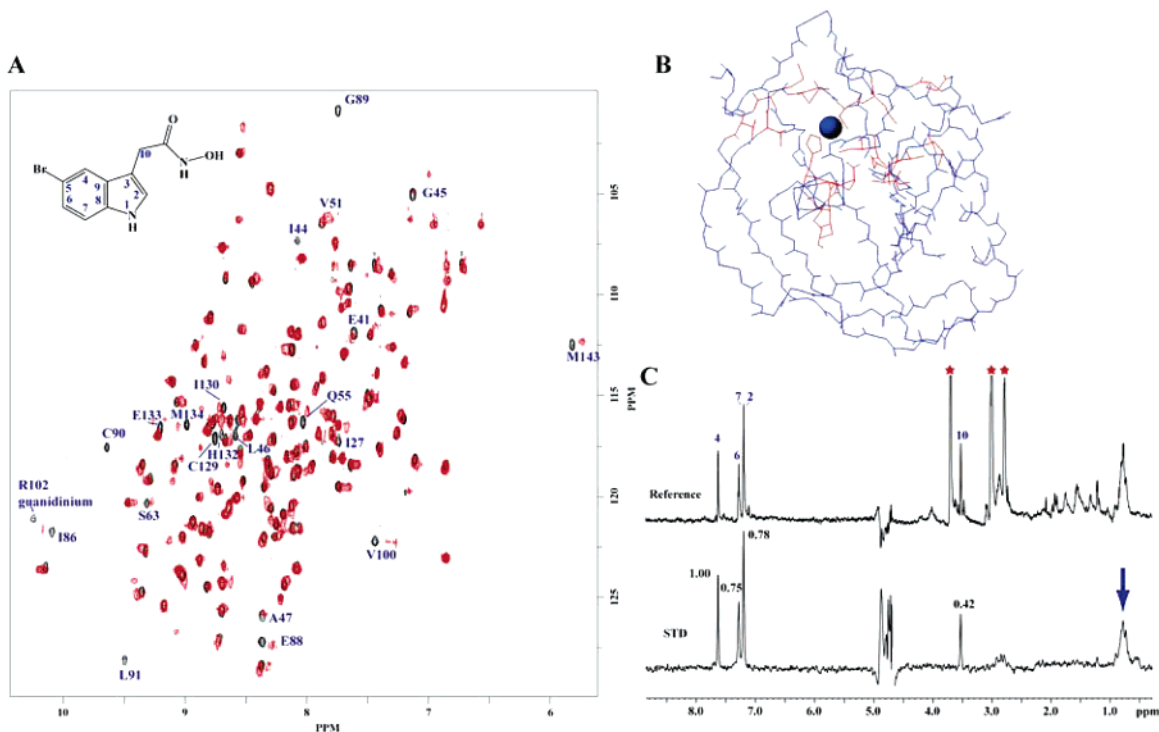
Figure 1. Mode by which **6b** binds to the active site pocket of PDF1B, as probed by NMR. (A) HSQC footprint of **6b** (top inset) on ^{15}N-labeled *E. coli* PDF. The reference spectrum is shown in black contours, and the spectrum in the presence of a stoichiometric amount of the compound is overlaid in red. Significantly perturbed amide groups are labeled according to NMR chemical shift assignments.[34] Similar footprints were obtained with several ID, including 5Br-indole. (B) 3D structure of *E. coli* PDF. The peptide chain is shown in blue. Amino acids in which the amide group NMR shift was perturbed by the binding of **6b** are shown in red (residues labeled in panel A). The catalytic metal cation is shown as a blue sphere. (C) NMR saturation transfer difference experiment (STD) showing the transfer of magnetization from *E. coli* PDF to **6b**. Upper trace shows the reference spectrum of the mixture. Peaks labeled with asterisks correspond to buffer signals. The numbered peaks correspond to signals originating from **6b**, as labeled in panel A. Lower trace shows STD signals. The arrow indicates the spectral region irradiated. Normalized STD intensities are indicated.

Scheme 1. ID Structure and Labeling: Chemical Structures of **6b**, Actinonin, and **18** and Their Main PDF Inhibition Properties

ID series	6b	Actinonin	18
	IC_{50} PDF2 = 0.01 μM IC_{50} mPDF = 130 μM	IC_{50} PDF2 = 0.01 μM IC_{50} mPDF = 0.03 μM	IC_{50} PDF2 = 0.3 μM IC_{50} mPDF = 83 μM

but not to mPDF. A medium-throughput screening system was used to identify such chemical groups by NMR. We used a pipetting robot connected to a flow-injection NMR probe and sequentially mixed peptide and non-peptide compounds with ^{15}N-labeled *E. coli* PDF (PDF1B), the resulting mixture being injected into the NMR spectrometer. Chemical shift perturbations were monitored by recording {[1]H−[15]N} heteronuclear single quantum correlation (HSQC) spectra, which were compared with control data obtained with the free enzyme, as previously described.[20,21] We selected compounds that caused resonance broadening or a shift in the HSQC protein spectrum. The amide groups concerned were identified and located on the three-dimensional (3D) structure of PDF1B (Figure 1A). Because compounds such as 5-bromoindole induced modifications of the {[1]H−^{15}N} 2D NMR map in a region corresponding to residues located in the S1′ pocket of the enzyme, the indole scaffold was selected from this screening. The effect of one of

the indole derivatives (ID; see Scheme 1 for labeling) is shown in Figure 1B. Similar strong perturbations of the HSQC spectrum were also observed with ID and PDF2. Reciprocal ligand-observed saturation transfer difference (STD) experiments[22] were carried out to obtain information about the mode of binding of these derivatives to both PDF1B (Figure 1C) and PDF2 (data not shown). The strongest STD effect was observed at R_4 of the indole moiety, and the weakest effect was that for the methylene group attached at position R_3. These results confirm that the indole group bound to both PDF1B and PDF2 and imply that position R_4 is buried the most deeply in the S′1 pocket.

Structure−Activity Relationship (SAR) Analysis of ID and 3D Modeling. Indole and 5-bromoindole had binding constants in the millimolar range, as shown by NMR titrations and/or PDF inhibition assays (Table 1). We tried to increase the potency of ID by introducing substituents at positions R_{1-6}. The synthesis

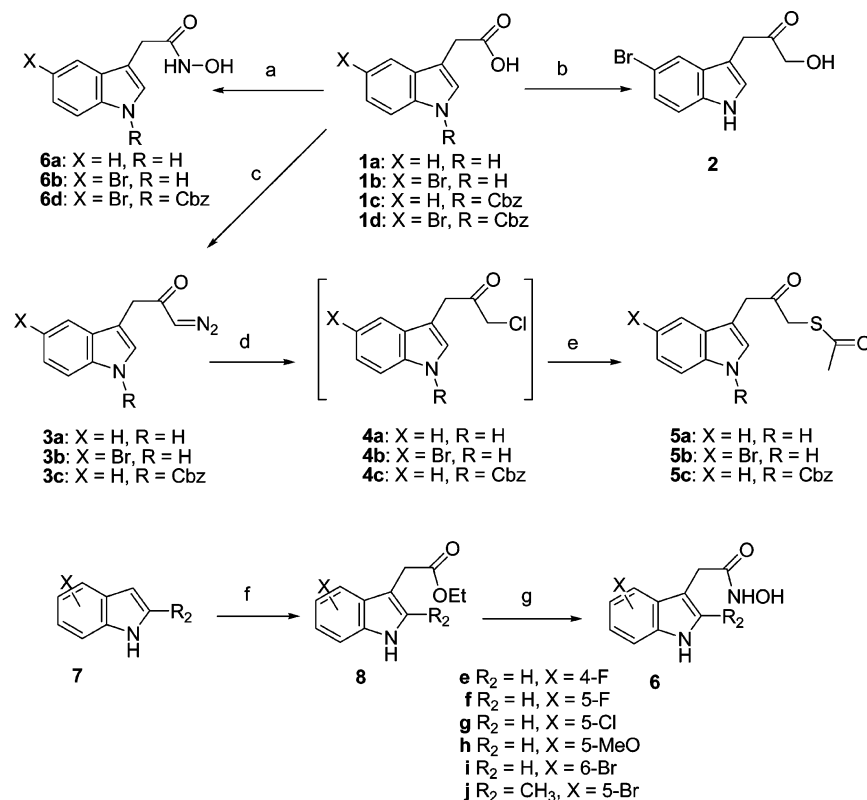**Table 1.** Structures and Associated IC_{50} Values with the Various Types of PDFs[b]

Compound	Chemical structure	IC_{50} (µM) mPDF (human)	IC_{50} (µM) AtPDF1A[a]	IC_{50} (µM) PDF1B	IC_{50} (µM) PDF2	MIC (µg/mL) E. coli JM101Tr	MIC (µg/mL) B. subtilis	Compound	Chemical structure	IC_{50} (µM) mPDF (human)	IC_{50} (µM) AtPDF1A[a]	IC_{50} (µM) PDF1B	IC_{50} (µM) PDF2	MIC (µg/mL) E. coli JM101Tr	MIC (µg/mL) B. subtilis
Actinonin		0.6	0.027	0.01	0.01	34	1.3	6f		ND	700	0.16	0.02	40	27
1a		ND	>1000	>1000	>1000	ND	ND	6g		600	250	0.08	0.015	25	13
1b		ND	>1000	380	60	ND	ND	6h		ND	>1000	9	0.33	>300	155
1c		ND	>1000	300	280	ND	ND	6i		250	250	0.21	0.03	ND	ND
2		ND	790	560	250	ND	ND	6j		450	450	3	0.1	>300	220
5a		ND	>1000	200	200	ND	ND	11		ND	>250	50	1	ND	ND
5b		ND	170	120	120	ND	ND	15		ND	500	6	0.4	ND	ND
5'b		ND	200	80	300	ND	ND	16		200	35	0.03	0.025	65	35
5c		ND	500	350	100	ND	ND	18		ND	83	0.044	0.3	>300	>300
6a		ND	>1000	1.4	0.3	115	160	20		ND	>1000	52	110	ND	ND
6b		360	130	0.035	0.013	6	3.1	21		ND	150	0.05	0.4	ND	ND
6d		ND	14	0.027	0.018	120	16								
6e		700	>1000	2	0.1	ND	ND								

[a] AtPDF1A corresponds to mitochondrial PDF1A from *Arabidopsis thaliana*, a mitochondrial PDF whose specific activity of the purified form is higher than that of mPDF and allows better assessment and inhibition properties of a mitochondrial PDF than mPDF.[8] [b] ND, not determined.

of 22 different ID is depicted in Schemes 2 and 3. Because phenyl side chains at P1′ are known to be poorly accepted by mPDFs[8,19] but strongly accepted by PDF1Bs,[17,21] we prepared the hydroxamic acid, hydroxylamine, and reverse hydroxamic acid of *N*-Boc-phenylalanine (compounds **18**, **20**, and **21**, respectively, Scheme 4). We first assessed the ability of all compounds to inhibit both PDF1B and PDF2. The hydroxamic and reverse hydroxamic acid were the most efficient functional groups introduced at R_3, in terms of binding (Table 1). SAR analysis was carried out with the hydroxamic acid derivatives by introducing various substituents at R_{4-6}. Because 5-Br indole derivative **6b** was the most potent inhibitor (Scheme 1), we also assessed the introduction of a methyl group at R_2 (**6j**) or of a benzyloxycarbonyl group at R_1 (**6d**). Whereas **6j** was one of the least potent inhibitors in this series, **6d** was as active as the

most potent compound **6b**, suggesting that the addition of bulky substitutions at R_1 has no effect on the affinity of ID. As expected from the characteristics of the S1′ pocket, none of the ID tested significantly inhibited mPDFs (Scheme 1 and Table 1). Finally, compounds **18** and **21** also efficiently inhibited PDF1B with only mild effects on mPDFs. However, these compounds, unlike ID, inhibited PDF2 only poorly (Scheme 1 and Table 1). They would therefore not be expected to display antibiotic activity against Gram-positive bacteria in vivo.

A 3D model of **6b** docked in the active site of PDF1B indicated a perfect fit within the S1′ pocket. The 5-Br group corresponded to the C_4 methyl group of the Met side chain (Figure S1 in Supporting Information), four-carbon chains being optimal for acceptance in the S1′ pocket.[17] In the model, position R_4 is locked deep inside the S1′ pocket, buried under the side

Scheme 2. Synthesis of Indole Derivatives: Hydroxyketones, Ketothioacetyl Derivatives, and Hydroxamic Acids[a]

6a: X = H, R = H
6b: X = Br, R = H
6d: X = Br, R = Cbz

1a: X = H, R = H
1b: X = Br, R = H
1c: X = H, R = Cbz
1d: X = Br, R = Cbz

2

3a: X = H, R = H
3b: X = Br, R = H
3c: X = H, R = Cbz

4a: X = H, R = H
4b: X = Br, R = H
4c: X = H, R = Cbz

5a: X = H, R = H
5b: X = Br, R = H
5c: X = H, R = Cbz

7   **8**

e R2 = H, X = 4-F
f R2 = H, X = 5-F
g R2 = H, X = 5-Cl
h R2 = H, X = 5-MeO
i R2 = H, X = 6-Br
j R2 = CH3, X = 5-Br

6

[a] (a) (1) HOBt, EDCI, NMM/DMF; (2) NH2OH·HCl/DMF; (b) (1) (COCl)2, DMF/THF; (2) C11H28O3Si3/dioxane; (3) HCl(g), dioxane, 80 °C; (c) (1) SOCl2/CH2Cl2, 40 °C; (2) CH2N2, diethyl ether/CH2Cl2, 0 °C; (d) HCl(g), diethyl ether, 0 °C; (e) KSAc/DMF; (f) (1) *n*-BuLi, ZnCl2/THF, 0 °C; (2) BrCH2COOEt/toluene; (g) NH2OH, ethanol, 80 °C.

Scheme 3. Synthesis of Hydroxylamines and Reverse Hydroxamic Acid Indole Derivatives[a]

12

7j   **9**   **10**   **11**

13   **14**   **15**   **16**
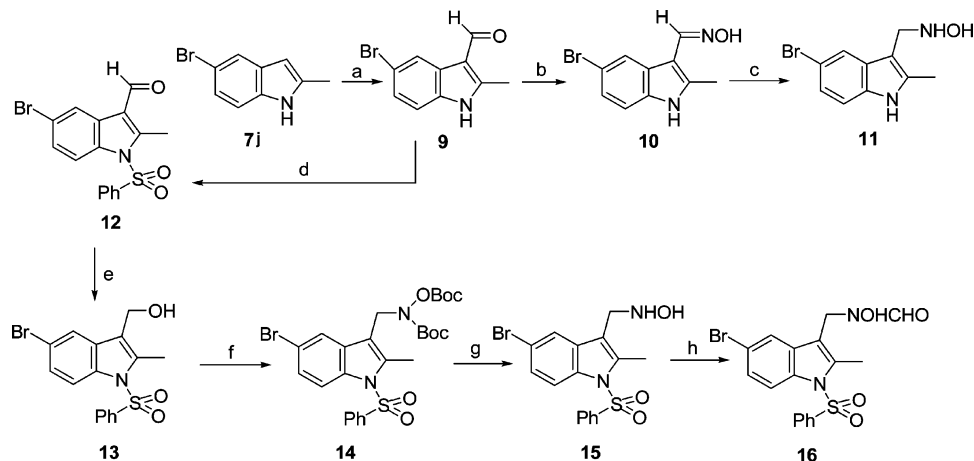
[a] (a) (1) POCl3, DMF; (2) NaOH; (b) NH2OH, HCl/pyridine; (c) NaBH3CN, HCl; (d) (1) NaH/THF; (2) PhSO2Cl; (e) NaBH4/ethanol; (f) (1) PPh3, NBS; (2) BocNH2OBoc, NaH /DMF; (g) (1) CF3COOH/CH2Cl2; (h) HCOOH, Ac2O/CH2Cl2.

chain of His132, consistent with the STD data. We cocrystallized **6b** with PDF1B. The difference between the electron density maps of the free protein and of the complex confirmed that the inhibitor bound to the active site according to the model proposed in Figure S1. These data suggest that the antibiotic activity of ID may target bacterial PDFs in vivo without inhibiting animal PDFs and causing apoptosis.

Like Actinonin, 6b Shows Slow, Tight Binding to PDF. The most potent PDFI show slow, tight binding to PDF.[23,24] Detailed kinetic analysis is required to characterize this process.[25] We studied and compared the binding mechanisms of **6b** and actinonin. When the reaction was triggered by adding

the enzyme (Figure S2A,B of Supporting Information), the initial rate of reaction decreased rapidly, reaching a minimum within 3 min, for both compounds. When the reaction was initiated by adding the substrate after incubating the enzyme with the inhibitor (Figure S2C,D), the kinetics of the reaction were linear over a long period of time (10 min) and the initial reaction rate corresponded to that reached after 3 min in the second phase of the experiment performed without prior incubation of enzyme and inhibitor. Thus, both actinonin and **6b** induced similar slow binding to PDF via a two-step mechanism (Figure S3A). The K_I value for the inhibitor/enzyme pre-equilibrium was ∼100 nM for both compounds, similar to previously reported values.[23]
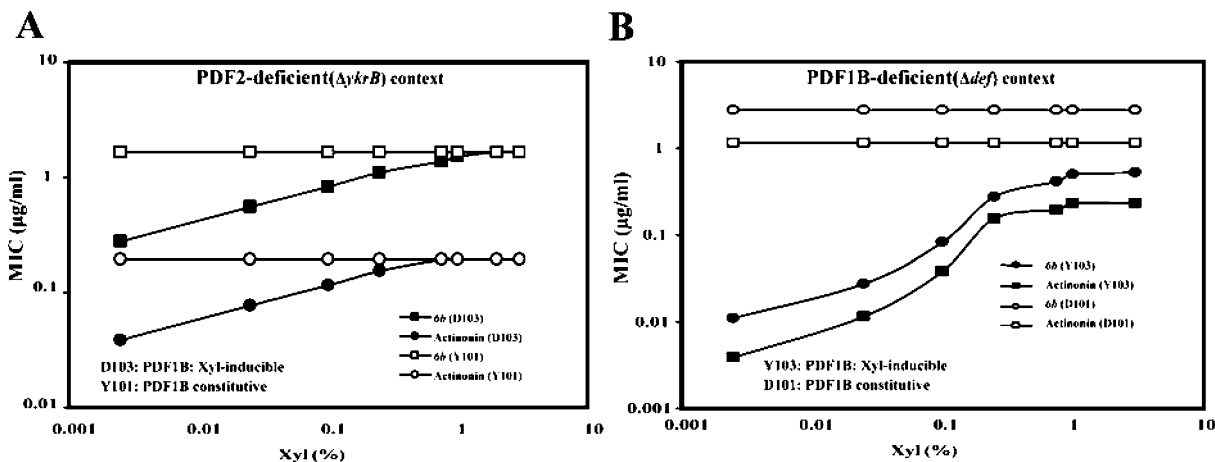
Figure 2. **6b** specifically targets both PDF types in vivo. The xylose-inducible Y103 and D103 strains of *B. subtilis* were cultured in the presence of various concentrations of L-xylose (Xyl) to increase intracellular PDF concentration.[27] Constitutive strains (Y101 and D101) were cultured under the same conditions for comparison. MIC values were determined for **6b** (black squares, 103 series; white squares, 101 series) and compared with those obtained for actinonin (black circles, 103 series; white circles, 101 series). (A) PDF2-deficient context. The *pdf1b* gene is either constitutively expressed (strain Y101) or inducible with L-xylose (strain D103). (B) PDF1B-deficient context. The *pdf2* gene is either constitutively expressed (strain D101) or inducible with L-xylose (strain Y103).
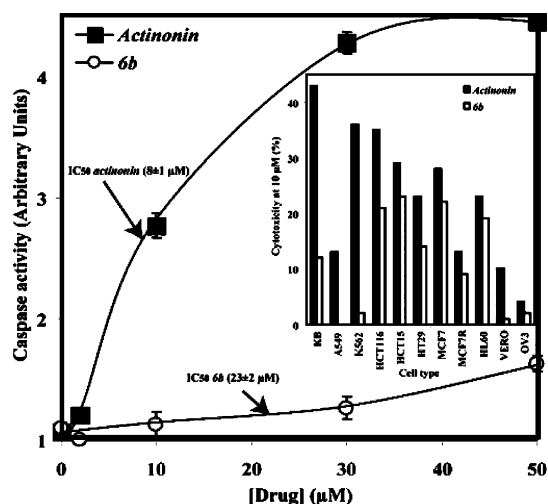

Figure 3. **6b** does not cause significant toxic effects by inducing apoptosis in human cells. Apoptosis in KB cells was assessed by measuring caspase induction. The inset shows the results of toxicity assays in the presence of 10 μM drug with various cell types.

The K_I^* value (Figure S3B,C) corresponded to the PDF concentration used in the assay, indicating tight binding. Because we could not use lower enzyme concentrations, this K_I^* value should be considered as a $K_I^*_{app}$ (Table 2). The constants for binding to PDF2 of both actinonin and **6b** were therefore determined using Henderson's method[26] (Figure S3D). The two compounds had similar K_I^*, in the nanomolar range (Table 2). However, compound **18**, the pseudopeptide analogue, displayed neither slow nor tight binding to PDF2. This accounts for the low IC$_{50}$ of compound **18** for PDF2 (Scheme 1). This suggests that **6b**, unlike **18**, is able to induce a change in the conformation of the protein. This property might be displayed by any potent PDFI. Because compound **6d** also displayed slow and tight binding, the ID series was considered a promising source of potent and specific PDFI.

ID Have Antibiotic Activity. We determined the antibiotic properties of certain ID. In *Bacillus subtilis*, the MIC of **6b** was similar to that of actinonin, in the μg/mL range, whereas that of **6d** was slightly higher (Table 3). We assessed the effects of **6b**, **6d**, and actinonin on two *B. subtilis* strain derivatives

Scheme 4. Synthesis of Pseudopeptide Derivatives[a]
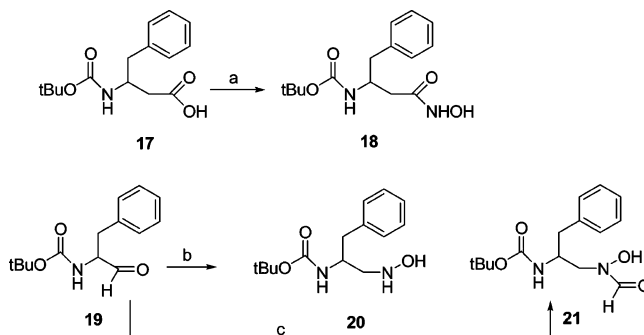
[a] (a) (1) HOBt, EDCI, NMM/DMF; (2) NH$_2$OH·HCl/DMF; (b) (1) NH$_2$OH, HCl/pyridine; (2) NaBH$_3$CN, CH$_3$COOH/methanol; (c) (1) PhCH$_2$NHOH·HCl/pyridine; (2) NaBH$_3$CN, CH$_3$COOH/methanol; (3) HCOOH, acetic anhydride; (4) H$_2$, Pd/C.

Table 2. Comparison of the Main Kinetic and Thermodynamic Parameters Describing PDF2 Inhibition by **6b** and Actinonin

parameter	actinonin[a]	**6b**[a]
K_I (nM)	185 ± 15^b	91 ± 9^c
$K_I^*_{app}$ (nM)	10 ± 1^d	15 ± 2^e
K_I^* (nM)	2.9 ± 0.8^f	5.6 ± 1.9^f
K_I/K_I^*	64 ± 7	16 ± 3
k_5 (s^{-1})[g]	0.075 ± 0.008	0.074 ± 0.008
k_6 (s^{-1})[h]	0.0011 ± 0.0003	0.0049 ± 0.0009
$t_{1/2}$ (min)[h]	10	2.4

[a] The PDF2 concentration used in the assay was 25 nM. The analysis in Figure S2D indicates that the active site enzyme concentration of our preparation was 11 ± 2 nM, i.e., 40−50% the initial enzyme concentration. [b] Derived from the curve shown in Figure S2B. [c] Derived from the curve shown in Figure S2C. [d] Derived from the curve shown in Figure S2B. [e] Derived from the curve shown in Figure S2C. [f] Derived from the curve shown in Figure S2D. [g] Derived from the curve shown in Figure S2E. [h] $k_6 = k_5/(K_I/K_I^* - 1)$ and $t_{1/2} = \log 2/k_5$.

(D101 and Y101), each with only one type of PDF (Table 3). We found that the MIC values of actinonin, **6b**, and **6d** followed similar trends, being lower in the *ykrB* (PDF2) gene-inactivated context. These results confirmed that *def* was less strongly expressed than *ykrB*[27] and suggested that **6b** and **6d** targeted both PDF1B and PDF2. The MIC of **6b** was half that of actinonin in *E. coli* (Table 3). In *E. coli*, actinonin is detoxified by the AcrAB-tolC efflux pump. We used a *tolC* mutant to

Table 3. In Vivo Antibiotic Activity of the ID Series[c]

bacterial strain		actinonin	6b	6d	6a	2	18	21
		MIC (µg/mL)						
E. coli	JM101Tr	32−64	4−8	120	114	>300	>300	>300
	K37	32−64	16−32	ND	ND	ND	ND	ND
	CAG1284	0.125−0.25	8−16	25	95	>300	32	120
B. subtilis	168[a]	1−2	2−4	16	160	>300	>300	>300
	D101[b]	1−2	2−4	12	150	>300	>300	>300
	Y101[b]	0.125−0.25	1−2	6	145	>300	8	9

[a] Identical results were obtained with MO3482. [b] Both strains were derived from 168.[27] D101 is deficient in PDF1B (*def* gene), the minor PDF in *B. subtilis*,[27] and Y101 is deficient in PDF2 (*ykrB* gene). [c] ND, not determined.

determine whether such efflux was involved in **6b** detoxification. The MIC of **6b** was only slightly lower in this mutant, whereas that of actinonin was lower than that in the wild type by a factor of 300. Thus, this efflux system detoxified ID less efficiently than actinonin. Compounds **2**, **6a**, **18**, and **21** had no antibiotic activity.

ID Specifically Target PDF in Vivo. We next assessed the specificity of PDF targeting by **6b** in vivo, using two *B. subilis* mutants in which (i) both the *ykrB* and *def* genes had been inactivated and (ii) a supplementary copy of one of the two PDF genes was placed under the control of the *XylR* promoter. Under these conditions, the synthesis of PDF1B or PDF2 from the gene concerned depends on L-xylose.[27] The MIC values of both actinonin and **6b** depended strongly on L-xylose concentration in both mutant strains (Figure 2). The range of induction was similar in both genetic contexts, with a plateau reached at the same concentration. Moreover, at concentrations 4 times the MIC (as indicated in Table 3), both actinonin and **6b** induced bacteriostatic activity in the first 4 h after drug addition. Finally, we determined the frequency with which resistance to **6b** and actinonin appeared in *B. subtilis*. Similar values (5×10^{-7}) were obtained for these two compounds, in keeping with previous reports for actinonin.[28] The resistant strains isolated on **6b** at 8 times the MIC showed (i) resistance to actinonin at 8 times the MIC and (ii) a decrease in doubling time by a factor of 3−8. Actinonin-resistant strains also proved to be resistant to **6b**. The resistant strains were sensitive to other antibiotics, consistent with the resistance being specific to the inhibited target, PDF. Resistance to **6b** and actinonin was consistent with the bypassing of PDF activity induced by Met-tRNA^{fMet} transformylase gene (*fmt*) inactivation.[28] The sequencing of a number of **6b**-resistant clones led to the identification of various mutations in *fmt*, all of which were predicted to lead to gene-function inactivation. Because the major fitness cost associated with this *fmt* inactivation conferring PDFI resistance can be compensated only partly by further mutations, at extremely low (10^{-14}) rates,[29] PDF may be considered a target of choice for new antibiotics. These data provide further evidence that the bacterial target of **6b**, like that of actinonin, is PDF.

ID Do Not Trigger Apoptosis. Actinonin has been reported to induce apoptosis in some cell lines, with cytotoxicity, and with IC$_{50}$ values in the range of 2−10 µM.[6,12,14,15] Lower levels of toxicity were observed with **6b** than with actinonin in various cell lines (Figure 3). Apoptosis was strongly induced by actinonin, as shown by the measurement of caspase activation in KB cells (Figure 3). At the IC$_{50}$ of the two compounds, actinonin induced apoptosis at least 10 times more strongly than **6b** in KB cells. At the IC$_{50}$ of actinonin in KB cells, **6b** gave negligible levels of apoptosis. Thus, ID fulfill in vivo the conditions imposed at the beginning of the study; they do not block mPDF because they do not trigger apoptosis, but they do have potent antibiotic activity.

Conclusions

We report here the first identification of a PDFI based on the medium-throughput NMR screening of different scaffolds, followed by SAR analysis, kinetic characterization, and mode-of-action determination and demonstration of antibiotic activity for the best compounds. The rationale for this screening was based on the structural analysis of mPDFs.[18] This made it possible to select PDFIs that inhibited both types of bacterial PDF, without significantly inhibiting mPDF. The mLogP value associated with **6b** (1.84) makes this molecule an excellent candidate drug. Further modification of ID, which currently have few substituents, could be used to improve their permeability and pharmacological properties, creating a new generation of antibiotics. In addition, some toxicity of **6b** was observed in a number of cell lines, although to a lesser extent than actinonin (Figure 3, inset). Because this effect is necessarily unrelated to mPDF inhibition, identification of the target(s) involved would be of strong interest to lower toxicity of future ID. Next developments will therefore include the determination of the inhibition capacities by ID of various human metallopeptidases such as matrix metalloproteases (MMPs) or angiotensin I converting enzyme (ACE), which are known to be slightly inhibited by PDFI such as BB-3497 and various hydroxamate derivatives of the actinonin series, including actinonin itself.[30,31]

Experimental Section

Protein Analysis. *Escherichia coli* PDF (PDF1B) and *Bacillus stearothermophilus* PDF2 (PDF2) were used as the representatives of the two bacterial PDF classes. They were purified in the presence of nickel to yield highly active Ni-PDF.[32] PDF activity was measured as previously described.[33] We monitored, at 37 °C, the absorbance at 340 nm of NADH ($\epsilon_M = 6300$ M^{-1} cm^{-1}), essentially as previously described.[33] Fo-Met-Ala-Ser (Bachem AG, Well-am-Rhein, Switzerland) was used as the substrate, and actinonin (Sigma, L'Isle d'Abeau Chesnes, France) was used as a PDF inhibitor for the purposes of comparison. The reaction was started by adding 5−15 µL of purified enzyme. All inhibitors were diluted in dimethylsulfoxide, and the final assay buffer contained 10% of this solvent. For the determination of all IC$_{50}$ values (IC$_{50}$ is the concentration giving 50% inhibition of enzyme activity), to prevent the effects associated with slow binding,[24,25] each inhibitor was incubated with the enzyme for 10 min at 25 °C before kinetic analysis, which was initiated by adding the substrate. ^{15}N-Labeled PDFs were produced as previously described.[34] NMR experiments were carried out with a Bruker Avance 600 MHz NMR spectrometer equipped with a 3 mm triple-resonance flow-injection probe. The probe was connected to a Gilson liquid handler controlled by the NMR console (Bruker BEST system). The injection protocol was as previously described.[35] For chemical shift perturbation experiments, 90 µL of 1 mM ^{15}N-labeled PDF1B was mixed with an equal volume of the tested ligand (3 mM), dissolved in the same buffer, in a 96-well plate. The mixture was refrigerated at 4 °C on a Gilson 242 Peltier rack before injection and HSQC experiments. The conditions for saturation transfer difference[22] experiments were similar except that the final PDF (unlabeled) and ligand concentrations were 20 µM and 1 mM, respectively. STD irradiation was carried out for 1 or 2 s, with the carrier set on the solid methyl protein (0.5 ppm), using a field strength $\gamma B_1/(2\pi)$ of 100 Hz.

Chemistry. All solvents and chemicals were purchased from SDS and Aldrich, respectively. DMF, THF, and CH$_2$Cl$_2$ were dried according to standard procedures and stored over 4 Å molecular sieves under argon. ^{1}H NMR spectra were recorded on a Bruker ARX-250 spectrometer, and chemical shifts were expressed in ppm downfield from TMS. IR spectra were obtained with a Perkin-Elmer Spectrum One FT-IR spectrometer equipped with a MIRacle single-reflection horizontal ATR unit (zirconium−selenium crystal). FAB and CI mass spectra were recorded at the ENS in Paris. Elemental analyses were carried out by the microanalysis service at Paris VI

University (France) or at Gif-Sur-Yvette (CNRS, France). Experiments performed under argon were run on a vacuum line. The various synthetic pathways for the products are depicted in Schemes 2−4. General procedures for the chemical syntheses of all compounds described are reported below, and elemental analysis results for target compounds are shown in Table S1 in Supporting Information.

3-Carboxymethylindol-1-carboxylic Acid Benzyl Ester (1c). A solution of 2-(indol-3-yl)acetic acid (500 mg, $M = 175.19$, 2.85 mmol) and LHMDS (1 M in THF, 6.27 mmol, 2.2 equiv, 6.27 mL) in freshly distilled THF (10 mL) was stirred at −78 °C under argon for 1 h. Benzyl chloroformate (505 μL, $M = 170.60$, $d = 1.195$, 3.42.mmoL, 1.2 equiv) was then added. The reaction mixture was stirred at −78 °C for 2 h, and solvents were then evaporated under vacuum. The residue was dissolved in water and extracted with diethyl ether. The aqueous layer was then acidified to pH 3 with aqueous 0.1 N HCl, resulting in the formation of 3-carboxymethylindol-1-carboxylic acid benzyl ester **1c** as a white precipitate, which was filtered off and washed with pentane (795 mg, yield of 90%). R_f (silica gel MerckF 254, CH_2Cl_2/CH_3OH, 9/1 v:v mixture) = 0.4. $T_f = 152$ °C. IR (cm^{-1}): 1728 and 1694 (ν_{CO}). ^{1}H NMR (250 MHz, DMSO-d_6): δ 3.77 (s, 2H), 5.53 (s, 2H), 7.29−7.66 (m, 8H), 7.74 (s, 1H), 8,14 (d, $J = 8.1$, 1H) ppm. CI-MS: $m/z = 327$ [M + NH$_4^+$], 100%. Expected values for $C_{18}H_{15}NO_4$: C, 69.89; H, 4.89; N, 4.53. Observed: C, 69.78; H, 5.00; N, 4.55.

3-Carboxymethyl-5-bromoindol-1-carboxylic Acid Benzyl Ester (1d). The same procedure applied to 2-(5-bromoindol-3-yl)-acetic acid (200 mg, $M = 254.09$, 0.787 mmol) yielded **1d** (280 mg, yield of 92%). R_f (silica gel CH_2Cl_2/CH_3OH, 9/1 v:v mixture) = 0.5, $T_f = 88$ °C. IR (cm^{-1}): 1729 and 1692 (ν_{CO}). ^{1}H NMR (250 MHz, acetone-d_6): δ 3.80 (s, 2H), 5.51 (s,2H), 7.15 (s,1H), 7.24−7.82 (m, 7H), 8.12 (d, $J = 8,1$, 1H), 11.16 (s, 1H) ppm. CI-MS: $m/z = 405$, 407 [M + NH$_4^+$], 40%; 388, 390 [M$^+$], 30%. Expected for $C_{18}H_{14}BrNO_4 \cdot 0.5H_2O$: C, 54.53; H, 3.87; N, 3.53. Observed: C, 54.67; H, 3.72; N, 3.44.

1-(5-Bromo-1H-indol-3-yl)-3-hydroxypropan-2-one (2). Oxalyl chloride (104 μL, $M = 126.93$, $d = 1.455$, 1.18 mmoL, 1.5 equiv) was added at 0 °C, under argon, to a solution (10 mL) of 2-(5-bromo-1H-indol-3-yl)acetic acid (200 mg, $M = 254.09$, 0.788 mmoL) in THF containing a few drops of DMF. The mixture was stirred at room temperature for 2 h, and the solvent was then evaporated under vacuum. Tris(trimethylsilyloxy)ethylene (675 μL, $M = 292.59$, $d = 0.885$, 1.94 mmoL, 2.3 equiv) was added, under argon, to the residue dissolved in 10 mL of dioxane. After the mixture was stirred at room temperature for 10 h, 10 mL of aqueous HCl (0.1 N) was added and the solution was heated at 80 °C for 30 min. NaCl was added, and the solution was extracted with diethyl ether. The organic layer was washed with brine, dried over MgSO$_4$, and evaporated to dryness under vacuum. After purification by column chromatography (silica gel, elution with CH_2Cl_2/CH_3OH, 95/5 v:v mixture), 1-(5-bromo-1H-indol-3-yl)-3-hydroxypropan-2-one **2** was obtained (45 mg, yield of 21%). R_f (silica gel, $CH_2Cl_2/$ CH_3OH, 9/1 v:v mixture) = 0.5. $T_f = 88$ °C. IR (cm^{-1}): 1702 (ν_{CO}). ^{1}H NMR (250 MHz, CDCl$_3$): δ 3.00 (s, 1H), 3.81 (s, 2H), 4.31 (s,2H), 7.15 (s,1H), 7.19−7.32 (m, 2H), 7.64 (s, 1H), 8.21 (s, 1H) ppm. CI-MS: $m/z = 285$, 287 [M + NH$_4^+$], 80%; 268, 270 [M$^+$], 100%. Expected for $C_{11}H_{10}BrNO_2$: C, 49.28; H, 3.76; N, 5.22. Observed: C, 49.10; H, 3.75; N, 5.17.

Thioacetic Acid S-[3-(Indol-3-yl)-2-oxopropyl] Ester (5a). Thionyl chloride (150 μL, $M = 118.97$, $d = 1.63$, 2.06 mmoL, 1.2 equiv) was added, under argon, to a solution (10 mL) of 2-(indol-3-yl)acetic acid (300 mg, $M = 175.19$, 1.72 mmoL) in CH$_2$Cl$_2$. The mixture was heated at 40 °C for 3 h, and the solvent was evaporated at low pressure. The residue was dissolved in CH$_2$Cl$_2$ (10 mL) and added to a freshly prepared solution of diazomethane in diethyl ether under argon via a syringe (10.4 mL, $C = 0.66$ M, 6.88 mmoL, 4 equiv). After being stirred at 0 °C for 4 h, the solution was evaporated under reduced pressure to give in a 95% yield the diazo compound **3a** as a yellow oil that was used without further purification. **3a**: R_f (silica gel, ethyl acetate/cyclohexane, 1/1 v:v mixture) = 0.65. IR (cm^{-1}): 2100 (ν_{CN}), 1726 (ν_{CO}). ^{1}H NMR (250

MHz, CDCl$_3$): δ 3.76 (s, 2H), 5.28 (s, 1H), 7.14−7.28 (m, 3H), 7.39 (d, $J = 7.8$, 1H), 7.48 (d, $J = 7.7$, 1H), 8.12 (s, 1H) ppm. CI-MS: $m/z = 217$ [M + NH$_4^+$], 50%; 200 ([M + H]$^+$), 30%. An etheral solution of HCl(g) (630 μL, $C = 6$ N, 3.78 mmoL, 2.2 equiv) was added to a solution (10 mL) of **3a** in diethyl ether. We added 5 mL of DMF, and diethyl ether was carefully evaporated. A solution (5 mL) of KSAc (432 mg, $M = 114.20$, 3.78 mmoL, 2.2 equiv) in DMF was added, via a syringe, under argon. The solution was stirred overnight at room temperature. Evaporation of the solvent under vacuum yielded **5a**, which was further purified by column chromatography, with elution with a 8/2 v:v mixture of ethyl acetate/cyclohexane (220 mg, yield of 52%). R_f (silica gel, ethyl acetate/cyclohexane, 1/1 v:v mixture) = 0.6. IR (cm^{-1}): 1788 (ν_{CO}). ^{1}H NMR (250 MHz, CDCl$_3$): δ 2.34 (s, 3H), 3.78 (s, 2H), 3.95 (s, 2H), 7.09−7.57 (m, 5H), 8.19 (s, 1H) ppm. CI-HRMS: expected for $C_{13}H_{14}NO_2S^+$ ([M + H]$^+$), 248.0445. Observed, 248.0448.

Thioacetic Acid S-[3-(5-Bromo-1H-indol-3-yl)-2-oxopropyl] Ester (5b). The same procedure applied to (5-bromoindol-3-yl)-acetic acid (300 mg, $M = 254.09$, 1.18 mmoL) gave 227 mg of thioacetic acid 5-[3-(5-bromo-1H-indol-3-yl)-2-oxopropyl] ester **5b**, giving a yield of 59%. R_f (silica gel, ethyl acetate/cyclohexane, 1/1 v:v mixture) = 0.5. ^{1}H NMR (250 MHz, CDCl$_3$): δ 2.36 (s, 3H), 3.78 (s, 2H), 3.92 (s, 2H), 7.13−7.29 (m, 3H), 7.72 (s, 1H), 7.48 (d, $J = 7.7$, 1H), 8.18 (s, 1H) ppm. CI-HRMS: observed for $C_{13}H_{13}$-BrNO$_2S^+$ ([M + H]$^+$), ^{79}Br 325.9850, ^{81}Br 327.9830; observed, ^{79}Br 325.9843, ^{81}Br 327.9837.

Diazo Compound 3b. 3b was isolated in a 95% yield. R_f (silica gel, cyclohexane/ethyl acetate, 3/7 v:v mixture) = 0.5. IR (cm^{-1}): 2101 (ν_{CN}), 1715 (ν_{CO}). ^{1}H NMR (250 MHz, CDCl$_3$): δ 3.75 (s, 2H), 5.68 (s, 1H), 7.22 (dd, $^3J = 8.5$, $^4J = 1.5$, 1H), 7.34 (s, 1H), 7.37 (d, $^3J = 8.5$, 1H), 7.75 (d, $^4J = 1.5$, 1H) ppm. CI-MS: $m/z = 278$, 280 [M$^+$], 60%; 250, 252 ([M − N$_2$]$^+$), 100%.

3-(3-Acetylsulfanyl-2-oxopropyl)indole-1-carboxylic Acid Benzyl Ester (5c). The same procedure applied to 3-carboxymethylindol-1-carboxylic acid benzyl ester (200 mg, $M = 309.32$, 0.647 mmoL) gave 178 mg of **5c**, corresponding to a yield of 72%. R_f (ethyl acetate/cyclohexane, 1/1 v:v mixture) = 0.6. ^{1}H NMR (250 MHz, acetone-d_6): δ 2.34 (s, 3H), 3.98 (s, 2H), 4.07 (s, 2H), 5.50 (s, 2H), 7.15−7.80 (m, 9H), 8.15 (d, $^4J = 1.5$, 1H) ppm. CI-HRMS: expected for $C_{21}H_{23}NO_4S^+$ [M + NH$_4^+$], 399.1379; observed, 399.1375.

Diazo Compound 3c. 3c was isolated with a yield of 91%. R_f (silica gel, ethyl acetate/cyclohexane, 1/1 v:v mixture) = 0.5. IR (cm^{-1}): 2102 (ν_{CN}), 1730, and 1636 (ν_{CO}). ^{1}H NMR (250 MHz, acetone-d_6): δ 3.78 (s, 2H), 5.50 (s, 2H), 5.82 (s, 1H), 7.26−7.69 (m, 8H), 7.70 (s, 1H), 8.17 (d, $J = 8$, 1H) ppm. CI-MS: $m/z = 351$ [M + NH$_4^+$], 100%.

2-(Indol-3-yl)-N-hydroxyacetamide (6a). A DMF solution (10 mL) of 2-(indol-3-yl)acetic acid (500 mg, $M = 175.19$, 2.85 mmol), 1-hydroxybenzotriazole (HOBT) (425 mg, $M = 135.13$, 3.14 mmol, 1.1 equiv), and 1-(3-dimethylaminopropyl)-3-ethylcarboxylimine hydrochloride, EDCI (602 mg, $M = 191.71$, 3.14 mmol, 1.1 equiv), was stirred under argon for 5 min. We then added N-methylmorpholine (NMM) (345 μL, $M = 101.15$, $d = 0.92$, 3.14 mmol, 1.1 equiv). The reaction mixture was stirred at room temperature for 2 h, and hydroxylamine hydrochloride (218 mg, $M = 69.5$, 3.14 mmol, 1.1 equiv) was added. The solution was stirred overnight, and the DMF was then evaporated under vacuum to give a yellow oil that was dissolved in ethyl acetate. This solution was successively washed with water and aqueous NaHCO$_3$. After the usual workup, solvent evaporation gave **6a** as a white solid (260 mg, yield of 60%). IR (cm^{-1}): 1638 (ν_{CO}). ^{1}H NMR (250 MHz, DMSO-d_6): δ 3.44 (s, 2H), 7.02 (t, $J = 7.1$, 1H), 7.12 (t, $J = 7.1$, 1H), 7.19 (s, 1H), 7.39 (d, $J = 7.8$, 1H), 7.62 (d, $J = 7.6$, 1H), 8.74 (s, 1H), 10.65 (s,1H), 11.85 (s, 1H) ppm. Expected for $C_{10}H_{10}N_2O_2$: C, 63.15; H, 5.30; N, 14.73. Observed: C, 62.96, H, 5.31, N, 14.63.

2-(5-Bromo-1H-indol-3-yl)-N-hydroxyacetamide (6b). Starting from (5-bromo-1H-indol-3-yl)acetic acid (200 mg, $M = 254.09$, 0.787 mmol), 116 mg of **6b** was obtained, with a yield of 55%. R_f (C18 silica gel, ethyl acetate/methanol, 1/1 v:v mixture) = 0.8. T_f

= 145 °C. IR (cm^{-1}): 3417 (ν_{OH}), 3213 (ν_{NH}), 1633 (ν_{CO}). ^{1}H NMR (250 MHz, DMSO-d_6): δ 3.49 (s, 1H), 7.20–7.44 (m, 3H), 7.87 (s, 1H), 8.86 (s, 1H), 10.59 (s, 1H), 11.14 (s, 1H) ppm. CI-MS: m/z = 270, 272 [M + H]$^+$, 100%. Expected for C$_{10}$H$_9$BrN$_2$O$_2$: C, 44.63; H, 3.37; N, 10.41. Observed: C, 44.52, H, 3.52; N, 10.45.

5-Bromo-3-hydroxycarbamoylmethylindole-1-carboxylic Acid Benzyl Ester (6d). Starting from 5-bromo-3-carboxymethylindol-1-carboxylic acid benzyl ester (120 mg, M = 388.21, 0.309 mmol), 50 mg of **6c** was obtained with a yield of 40%. IR (cm^{-1}): 1650 and 1690 (ν_{CO}). ^{1}H NMR (250 MHz, DMSO-d_6): δ 3.40 (s, 2H), 5.56 (s, 2H), 7.45–8.10 (m, 9H), 8.95 (s, 1H), 10.75 (s, 1H) ppm. Expected for C$_{18}$H$_{15}$BrN$_2$O$_4$: C, 53.62; H, 3.75; N, 6.95. Observed: C, 53.73; H, 3.54; N, 7.11.

(4-Fluoro-1H-indol-3-yl)acetic Acid Ethyl Ester (8e). To a cooled solution of 4-fluoro-1H-indole **7e** (M = 135.05, 300 mg, 2.22 mmol) in 3.3 mL of THF, we added 1.39 mL (2.22 mmol) of 1.6 M n-BuLi in hexane, keeping the solution below 0 °C with an ice bath. After 15 min, 2.22 mL of 1 N ZnCl$_2$ in diethyl ether was added. The cooling bath was removed, and the mixture was stirred for 24 h. The solvent was then evaporated under vacuum to give a wax, which was further dissolved in anhydrous toluene (3.3 mL). Ethyl 2-bromoacetate (246 μL, 2.22 mmol) was added, and the solution was stirred for 24 h. The mixture was then acidified with 1 N HCl and poured into ethyl acetate. The organic layer was washed with brine and dried over MgSO$_4$. The ester was subjected to chromatography on silica gel, eluting with 10% ethyl acetate/cyclohexane to give 158 mg (32%) of **8e**. ^{1}H NMR (250 MHz, acetone-d_6): δ 1.24 (t, J = 7, 3H), 3.88 (s, 2H), 4.16 (q, J = 7, 2H), 6.71 (dd, $^3J_{HF}$ = 11, $^3J_{HH}$ = 8, 1H), 7.06 (td, $^3J_{HH}$ = 8, $^4J_{HF}$ = 5.4, 1H), 7.23 (d, J = 8, 1H), 7.28 (d, $^5J_{HF}$ = 1.9, 1H), 10.34 (s, 1H) ppm.

2-(4-Fluoro-1H-indol-3-yl)-N-hydroxyacetamide (6e). NH$_2$OH·HCl (497 mg, 7.15 mmol) was added as a powder to 6.4 mL of a 1 M solution of sodium ethoxide in ethanol. This solution was added to an ethanol solution (10 mL) of the ester **8e** (158 mg, 0.715 mmol, M = 221.03). The mixture was stirred under argon at 80 °C for 24 h. After the mixture was cooled and the solvent was evaporated under vacuum, the residue was dissolved in ethyl acetate. This organic layer was washed with brine, aqueous NaHCO$_3$, 0.1 N HCl, and finally with brine and dried over MgSO$_4$. After evaporation under vacuum, the hydroxamic acid **6e** was dissolved in a 1:1 mixture of acetone/cyclohexane. Slow evaporation of acetone at low pressure gave 75 mg of **6e** as a white solid (51%). IR (cm^{-1}): 3354 (ν_{NH}), 3280 (ν_{OH}), 1631 (ν_{CO}). ^{1}H NMR (250 MHz, acetone-d_6): δ 3.72 (s, 2H), 6.70 (dd, $^3J_{HF}$ = 11, $^3J_{HH}$ = 8, 1H), 7.05 (td, $^3J_{HH}$ = 8, $^4J_{HF}$ = 5.4, 1H), 7.22 (d, J = 8, 1H), 7.28 (s, 1H), 10.00 (s, 1H), 10.43 (s, 1H). CI-HRMS: expected for C$_{10}$H$_{13}$N$_3$O$_2$F ([M + NH$_4$]$^+$), 226.0992; observed 226.0991.

(5-Fluoro-1H-indol-3-yl)acetic Acid Ethyl Ester (8f). We obtained 91 mg of the ester **8f** (yield of 44%) from 125 mg of 5-fluoro-1H-indole (**7f**) (M = 135.05, 0.926 mmol). ^{1}H NMR (250 MHz, acetone-d_6): δ 1.24 (t, J = 7.2, 3H), 3.74 (s, 2H), 4.13 (q, J = 7.2, 2H), 6.92 (t, J = 9, 1H), 7.30 (d, J = 9, 1H), 7.38 (m, 2H), 10.21 (s, 1H) ppm.

2-(5-Fluoro-1H-indol-3-yl)-N-hydroxyacetamide (6f). Starting from 91 mg of the ester **8f** (M = 221.23, 0.41 mmol), we obtained 21 mg (yield of 25%) of the hydroxamic acid **6f** (M = 208.19). IR (cm^{-1}): 3360 (ν_{NH}), 3175 (ν_{OH}), 1625 (ν_{CO}). ^{1}H NMR (250 MHz, acetone-d_6): δ 3.57 (s, 2H), 6.91 (td, $^3J_{HF}$ = $^3J_{HH}$ = 9.3, $^4J_{HH}$ = 2.3, 1H), 7.33–7.41 (m, 3H), 8.00 (s, 1H), 10.08 (s, 1H), 10.22 (s, 1H) ppm. CI-HRMS: expected for C$_{10}$H$_{10}$N$_2$O$_2$F ([M + H$^+$]), 209.0726; observed 209.0720.

(5-Chloro-1H-indol-3-yl)acetic Acid Ethyl Ester (8g). We obtained 198 mg of the ester **8g** (yield of 43%) from 300 mg of 5-chloro-1H-indole (**7g**) (M = 151.60, 1.98 mmol). ^{1}H NMR (250 MHz, acetone-d_6): δ 1.24 (t, J = 7, 3H), 3.77 (s, 2H), 4.14 (q, J = 7, 2H), 7.24 (d, J = 8.5, 1H), 7.35–7.40 (m, 2H), 7.79 (s, 1H), 10.33 (s, 1H) ppm.

2-(5-Chloro-1H-indol-3-yl)-N-hydroxyacetamide (6g). Starting from 198 mg of the ester **8g** (M = 233.26, 0.85 mmol), we obtained 194 mg (yield of 95%) of the hydroxamic acid **6g** (M = 224.64).

IR (cm^{-1}): 3348 (ν_{NH}), 3190 (ν_{OH}), 1625 (ν_{CO}). ^{1}H NMR (250 MHz, acetone-d_6): δ 3.59 (s, 2H), 7.10 (d, J = 8.5, 1H), 7.35 (s, 1H), 7.41 (d, J = 8.5, 1H), 7.67 (s, 1H), 10.00 (s, 1H), 10.29 (s, 1H) ppm. CI-HRMS: expected for C$_{10}$H$_{10}$N$_2$O$_2$Cl ([M + H$^+$]), 225.0431 (100%), 227.0461 (33%); observed 225.0432 (100%), 227.0413 (32.4%).

(5-Methoxy-1H-indol-3-yl)acetic Acid Ethyl Ester (8h). We obtained 219 mg of the ester **8h** (yield of 46%) from 300 mg of 5-methoxy-1H-indole **7h** (M = 147.18, 2.04 mmol). ^{1}H NMR (250 MHz, acetone-d_6): δ 1.23 (t, J = 7, 3H), 3.73 (s, 2H), 3.82 (s, 3H), 4.15 (q, J = 7, 2H), 6.79 (d, J = 8.5, 1H), 7.11 (s, 1H), 7.26–7.32 (m, 2H), 9.97 (s, 1H) ppm.

2-(5-Methoxy-1H-indol-3-yl)-N-hydroxyacetamide (6h). Starting from 219 mg of the ester **8g** (M = 233.26, 0.94 mmol), we obtained 90 mg (yield of 43%) of the hydroxamic acid **6h** (M = 220.22). IR (cm^{-1}): 3307 (ν_{NH}), 3160 (ν_{OH}), 1620 (ν_{CO}). ^{1}H NMR (250 MHz, acetone-d_6): δ 3.57 (s, 2H), 3.81 (s, 3H), 6.77 (dd, ^3J = 8.8, ^4J = 2.3, 1H), 7.15 (d, J = 2.3, 1H), 7.22 (s, 1H), 7.28 (d, J = 8.8, 1H), 7.93 (s, 1H) ppm, 10.04 (s, 1H). HRMS: expected for C$_{11}$H$_{13}$N$_2$O$_3$ ([M+H$^+$]), 221.0926; observed 221.0928.

(6-Bromo-1H-indol-3-yl)acetic Acid Ethyl Ester (8i). We obtained 192 mg of the ester **8i** (yield of 45%) from 300 mg of 6-bromo-1H-indole (**7i**) (M = 196.05, 1.53 mmol). ^{1}H NMR (250 MHz, DMSO-d_6): δ 1.23 (t, J = 7.2, 3H), 3.76 (s, 2H), 4.13 (q, J = 7.2, 2H), 7.19 (dd, ^3J = 8.5, ^4J = 1.5, 1H), 7.34 (s, 1H), 7.55 (d, J = 8.5, 1H), 7.62 (d, J = 1.5, 1H), 10.28 (s, 1H) ppm.

2-(6-Bromo-1H-indol-3-yl)-N-hydroxyacetamide (6i). Starting from 192 mg of the ester **8i** (M = 282.16, 0.68 mmol), we obtained 136 mg (yield of 74%) of the hydroxamic acid **6i** (M = 269.09). IR (cm^{-1}): 3335 (ν_{NH}), 3230 (ν_{OH}), 1615 (ν_{CO}). ^{1}H NMR (250 MHz, acetone-d_6): δ 3.60 (s, 2H), 7.17 (dd, ^3J = 8.5, ^4J = 1.5, 1H), 7.30 (s, 1H), 7.6 (m, 2H), 8.0 (s, 1H), 10.0 (s, 1H), 10.27 (s, 1H) ppm. CI-HRMS: expected for C$_{10}$H$_{10}$N$_2$O$_2$^{79}Br ([M + H$^+$]), 290.9745; observed 290.9743.

2-(5-Bromo-2-methyl-1H-indolyl)acetic Acid Ethyl Ester (8j). We obtained 201 mg of the ester **8j** (yield of 48%) from 300 mg of 5-bromo-2-methyl-1H-indole **7j** (M = 210.06, 1.43 mmol). ^{1}H NMR (250 MHz, acetone-d_6): δ 1.18 (t, J = 7, 3H), 2.33 (S, 3H), 3.66 (s, 2H), 4.06 (q, J = 7, 2H), 7.10 (d, J = 8, 1H), 7.22 (d, J = 8, 1H), 7.56 (s, 1H), 10.11 (s, 1H) ppm.

2-(5-Bromo-2-methyl-1H-indolyl)-N-hydroxyacetamide (6j). Starting from 201 mg of the ester **8j** (M = 296.16, 0.68 mmol), we obtained 160 mg (yield of 83%) of the hydroxamic acid **6j** (M = 283.12). IR (cm^{-1}): 1690 (ν_{CO}). ^{1}H NMR (250 MHz, acetone-d_6): δ 2.44 (s, 3H), 3.69 (s, 2H), 7.14 (d, J = 8.4, 1H), 7.26 (d, J = 8.4, 1H), 7.67 (s, 1H), 10.20 (s, 1H) ppm. CI-HRMS: expected for C$_{11}$H$_{14}$N$_2$O$_2$^{79}Br ([M + 3H]$^+$), 285.0239; observed 285.0234.

5-Bromo-2-methyl-1H-indole-3-carbaldehyde (9). POCl$_3$ (267 μL, 2.86 mmoL, d = 1.64) was added under argon at 0 °C to a solution of 5-bromo-2-methyl-1H-indole **7j** (500 mg, 2.38 mmol) in 5 mL of DMF. This mixture was stirred at room temperature overnight, and 2 mL of 2 N aqueous NaOH was then added. The solution was stirred for 2 h. It was then poured into ethyl acetate. After the mixture was washed with water, dried, and evaporated to dryness, 526 mg of **9** was isolated as a white solid (yield of 93%). IR (cm^{-1}): 1628 ($\nu_{C=O}$). ^{1}H NMR (250 MHz, acetone-d_6): δ 2.78 (s, 3H), 7.33 (d, ^3J = 8.45, 1H), 7.36 (d, ^3J = 8.45, 1H), 8.33 (s, 1H), 10.15 (s, 1H), 11.04 (s, 1H) ppm. CI-MS: m/z = 255, 257 [M + NH$_4$$^+$], 85%; 238–240, [M$^+$], 100%. Expected for C$_{10}H_8$BrNO: C, 50.45; H, 3.39; N, 5.88. Observed: C, 50.42, H, 3.49; N, 5.87.

5-Bromo-2-methyl-1H-indole-3-carbaldehydeoxime (10). NH$_2$OH·HCl (70 mg, 1.01 mmol) was added to a solution of **9** (200 mg, 0.84 mmoL) in 5 mL of pyridine. The solution was stirred at room temperature for 5 h and then evaporated to dryness. The residue was dissolved in ethyl acetate, and the resulting solution was successively washed with 1 N HCl and brine and dried over MgSO$_4$. The solvent was evaporated, and 210 mg of **10** was isolated as a yellow oil in quantitative yield. IR (cm^{-1}): 1622 ($\nu_{C=N}$). ^{1}H NMR (250 MHz, acetone-d_6): δ 2.53 (s, 3H), 7.2–7.35 (m, 2H), 7.80 (s, 1H), 8.32 (s, 1H), 9.69 (s, 1H), 10.49 (s, 1H) ppm. Expected

for $C_{10}H_9BrN_2O \cdot 0.25H_2O$: C, 46.63; H, 3.72; N, 10.87. Observed: C, 46.69; H, 3.66; N, 10.58.

N-[2-(5-Bromo-2-methyl-1H-indole-3-yl)methyl]hydroxylamine (11). To a 10 mL solution of (10) (110 mg, 0.43 mmol) in methanol, we added a few crystals of methyl orange followed by a few drops of an ethanolic solution of HCl(g) (2 N). The solution turned reddish purple. The red color of the solution was maintained by adding HCl, and an amount of 2 equiv of NaBH$_3$CN (55 mg, 0.86 mmol) in 5 mL of THF was added. The solution was stirred. A few hours later, the red color was stable and the solution was left with stirring overnight. The solvent was evaporated, the residue was dissolved in 5 mL of methanol, and 5 mL of water was added. The pH was adjusted to 9 with 1 N aqueous NaOH. This solution was extracted with CH$_2$Cl$_2$. After the usual workup, **11** (110 mg) was isolated as a yellow oil in a quantitative yield and was characterized without further purification. ^{1}H NMR (250 MHz, acetone-d_6): δ 2.51 (s, 3H), 5.16 (s, 2H), 7.1−7.3 (m, 2H), 8.10 (s, 1H), 10.34 (s, 1H) ppm. CI-MS: m/z = 255, 257 [M$^+$], 30%; 224, 226 ([M − NHOH]$^+$), 100%. Expected for $C_{10}H_{11}BrN_2O$: C, 47.08; H, 4.35; N, 10.98. Observed: C, 46.97; H, 4.51; N, 11.13.

5-Bromo-2-methyl-1-(phenylsulfonyl)-1H-indole-3-carbaldehyde (12). A solution of 5-bromo-2-methyl-1H-indole-3-carbaldehyde **9** (500 mg, 2.10 mmol) was added at 0 °C under argon to a suspension of NaH (110 mg, 4.62 mmol, 2.2 equiv) in 10 mL of THF. The solution was stirred for 1 h, and a solution of benzenesulfonyl chloride (320 μL, 2.52 mmol, 1.2 equiv) was added. The mixture was stirred overnight at room temperature. We then added 50 mL of water and extracted the solution with ethyl acetate. The organic layer was washed successively with 0.1 N HCl, aqueous NaHCO$_3$, and brine and dried over MgSO$_4$. Filtration over Celite and evaporation gave 700 mg of **12** (95% yield) after recrystallization from a pentane/acetone mixture. ^{1}H NMR (250 MHz, acetone-d_6): δ 3.05 (s, 3H), 7.57 (dd, ^3J = 8.9, ^4J = 2.1, 1H), 7.6−8.0 (m, 5H), 8.19 (d, J = 8.9, 1H), 8.41 (d, J = 2.1, 1H), 10.32 (s, 1H) ppm. CI-MS: m/z = 378, 380 [M$^+$], 100%.

2-(5-Bromo-2-methyl-1-(phenylsulfonyl)-1H-indol-3-yl)ethanol (13). To a solution of **12** (700 mg, 1.85 mmol) in 10 mL of methanol, we added a solution of NaBH$_4$ (84 mg, 2.22 mmol) in 10 mL of methanol. After the mixture was stirred for 6 h at room temperature, the solution was poured into ethyl acetate and washed with water and brine. The organic layer was dried over MgSO$_4$, and the solvent was evaporated under vacuum. The alcohol was subjected to silica gel chromatography, with elution with cyclohexane/ethyl acetate, 70/30, yielding 700 mg of **13** in quantitative yield as a pale-yellow powder. ^{1}H NMR (250 MHz, acetone-d_6): δ 2.64 (s, 3H), 4.02 (s, 1H), 4.72 (s 2H), 7.45 (dd, ^3J = 8.9, ^4J = 2, 1H), 7.83 (d, J = 2, 1H), 7.6−8.0 (m, 5H), 8.13 (d, J = 8.9, 1H) ppm. CI-MS: m/z = 380, 382 [M$^+$], 100%.

tert-Butyl 2-(5-Bromo-2-methyl-1-(phenylsulfonyl)-1H-indol-3yl)methyl(tert-butoxycarbonyloxy)carbamate (14). To a solution of **13** (220 mg, 0.58 mmol) in 10 mL of THF, we successively added, at room temperature under argon, PPh$_3$ (1.1 equiv, 167 mg, 0.64 mmol). We stirred the mixture for 15 min and then added N-bromosuccinimide (1.1 equiv, 113 mg, 0.64 mmol). The mixture was stirred at room temperature overnight. The bromo derivative was not isolated and was subsequently tested in this solution. A solution of N,O-bis(tert-butoxycarbonyl)hydroxylamine (135 mg, 0.58 mmol) in 5 mL of DMF previously stirred for 15 min with NaH (1.1 equiv, 15 mg) was added to the bromo derivative. The resulting solution was stirred for 2 h. After the addition of CH$_2$Cl$_2$, the solution was washed with water, aqueous NH$_4$Cl, and brine and dried over MgSO$_4$. The solvent was evaporated, and the residue was subjected to silica gel chromatography, with elution in CH$_2$Cl$_2$/C$_6$H$_{12}$, 70/30 and 80/20, giving 150 mg of **14** (yield of 44%). ^{1}H NMR (250 MHz, acetone-d_6): δ 1.35 (s, 9H), 1.49 (s, 9H), 2.67 (s, 3H), 4.87 (s, 2H,), 7.47 (dd, ^3J = 8.8, ^4J = 1.8, 1H), 7.63 (m, 3H), 7.78 (d, J = 1.8, 1H), 7.9 (d, J = 7.5, 2H), 8.13 (d, J = 8.8, 1H) ppm. CI-MS: m/z = 612, 614 [M$^+$], 100%.

N-((5-Bromo-2-methyl-1(phenylsulfonyl)-1H-indol-3-yl)methyl)hydroxylamine (15). We added 775 μL of trifluoroacetic acid (40 equiv) to a solution of **14** (150 mg, 0.25 mmol) in 10 mL of

CH$_2$Cl$_2$. The solution was stirred for 2 h at 0 °C under argon, then washed with water and aqueous NaHCO$_3$ and dried over MgSO$_4$. Filtration and evaporation at low pressure gave 80 mg of **15**, which was tested without further purification because of the instability of this molecule during silica gel chromatography. ^{1}H NMR (250 MHz, CD$_2$Cl$_2$): δ 8.13 (d, J = 9, 1H), 7.83 (d, J = 7.4, 2H), 7.73 (d, J = 1.7, 1H), 7.6 (m, 4H), 4.47 (s, 2H), 3.4 (s, 1H), 2.69 (s, 3H). CI-HRMS: expected for $C_{16}H_{14}O_3N_2BrS$ ([M − H]$^+$), 392.9909 (96%), 394.9889 (100%); observed 392.9911 (24.7%), 394.9895 (24.2%).

N-(1-Benzenesulfonyl-5-bromo-2-methyl-1H-indol-3-ylmethyl)-N-hydroxyformamide (16). Formic acid (3.77 mL, 0.1 mol) was added dropwise at 0 °C to acetic anhydride (9.45 mL, 0.1 mol). The mixture was then heated at 50 °C for 2 h and left to cool to room temperature. We added **15** (80 mg, 0.2 mmol) dissolved in 10 mL of CH$_2$Cl$_2$ dropwise, at room temperature, to this solution. The mixture was stirred overnight, and evaporation of the solvent under vacuum gave an oil, which was subjected to silica gel chromatography, with elution with CH$_2$Cl$_2$/C$_6$H$_{12}$, 99.5/0.5 (v:v mixture) in the presence of a few drops of acetic acid. Following evaporation, we obtained 50 mg of **16** (yield of 60%) upon precipitation from an ether solution into pentane. ^{1}H NMR (250 MHz, acetone-d_6): δ 2.72 (s, 3H), 4.81 (s, 2H), 7.47 (dd, ^3J = 8.8, ^4J = 1.9, 1H), 7.63 (t, J = 7.5, 2H), 7.73 (d, J = 7.5, 1H), 7.8 (d, J = 1.9, 1H), 7.94 (d, J = 7.5, 2H), 8.13 (d, J = 8.8, 1H), 8.35 (s, 1H), 9.10 (s, 1H) ppm. FAB$^+$-MS: 423, 425 ([M + H]$^+$), 10%; 461, 463 ([M + NH$_4^+$]), 10%. CI-HRMS: expected for $C_{17}H_{19}O_4N_3$-BrS ([M + NH$_4^+$]), 440.0280 (95.6%), 442.0260 (100%); observed 440.0292 (86.4%), 442.0247 (92.9%).

(1-Hydroxycarbamoylmethyl-2-phenylethyl)carbamic Acid tert-Butyl Ester (18). We prepared 50 mg of **18** with a 55% yield, following the usual procedure for hydroxamic acid synthesis starting from 3-tert-butoxycarbonylamino-4-phenylbutyric acid **17** (0.308 mmoL, M = 279.33, m = 86 mg). ^{1}H NMR (250 MHz, DMSO-d_6): δ 1.36 (s, 9H), 2.16 (m, 2H), 2.72 (m, 2H), 3.99 (m, 1H), 6.71 (d, J = 8.6, 1H), 7.19−7.35 (m, 5H), 8.83 (s, 1H), 10. 40 (s, 1H) ppm. Expected for $C_{14}H_{20}N_2O_4 \cdot 0.25H_2O$: C, 60.29; H, 7.59; N, 9.37. Observed: C, 60.19; H, 7.38; N, 9.58.

(1-Hydroxyaminomethyl-2-phenylethyl)carbamic Acid tert-Butyl Ester (20). Compound **20** was prepared from (1-formyl-2-phenylethyl)carbamic acid tert-butyl ester **19** following the same procedure as for **11**. The product was purified by flash chromatography over silica gel (95:5 CH$_2$Cl$_2$/AcOEt) to give a white solid (45%). ^{1}H NMR (250 MHz, CDCl$_3$): δ 1.4 (s, 9H), 2.6−2.7 (m, 1H), 2.8 (d, J = 6.7, 2H), 3.1−3.3 (m, 1H), 4.1−4.2 (m, 1H), 4.5−4.6 (m, 1H), 7.2−7.5 (m, 7H). Expected for $C_{14}H_{22}N_2O_3$: C, 63.13; H, 8.32; N, 10.51. Observed: C, 63.17; H, 8.14; N, 10.43.

(1-Hydroxycarbamoylmethyl-2-phenylethyl)carbamic Acid tert-Butyl Ester (21). Compound **21** was synthesized as described[36] from (1-formyl-2-phenylethyl)carbamic acid tert-butyl ester **19**. IR (cm^{-1}): 1682 (ν_{CO}). ^{1}H NMR (250 MHz, CDCl$_3$): δ 1.38 (s, 1H), 2.83 (d, J = 6.7, 2H), 3.08−4.01 (m, 2H), 4.19 (m, 1H), 4.61 (d, J = 3.9, 1H), 7.15−7.80 (m, 5H), 8.32 (s, 1H), 8.85 (s, 1H). Expected for $C_{15}H_{22}N_2O_4 \cdot 0.2H_2O$: C, 60.47; H, 7.58; N, 9.40. Observed: C, 60.67; H, 7.57; N, 9.31.

Microbiology. Two wild-type *Bacillus subtilis* strains were used: MO3482, a prototrophic *skin* prophage-cured derivative of JH642, and 168 (*trpC2*).[37] Strains Y101 ($\Delta ykrB$::nm, *trpC2*) and D101 (Δdef::nm, *trpC2*) were derived from 168.[27] Two 168 derivatives (one in which both wild-type PDF loci (*def* and *ykrB*) were deleted and another in which one PDF locus was conditionally expressed under the control of L-xylose) were used:[27] Y103 (Δdef::nm, $\Delta ykrB$::erm, $\Delta thrC$::xylR-P$_{xylA}$-ykrB-spc, *trpC2*) and D103 (Δdef::erm, $\Delta ykrB$::nm, $\Delta thrC$::xylR-P$_{xylA}$-def-spc, *trpC2*). *E. coli* strains K37 (*galK*), JM101Tr (*galK*, *rpsL*, *recA56*, *srl*-300::Tn*10*), and CAG1284 (λ^-, *tolC210*::Tn*10*, *rph*-) have been described elsewhere.[38−40] Drug susceptibility was determined by culturing an inoculum containing $(1−4) \times 10^4$ CFU. The inoculum was cultured for 18 h at 37 °C in 3 mL of Mueller−Hinton broth medium (Sigma) in the presence of various dilutions of the drug. The MIC value obtained corresponds to the lowest concentration of the drug

at which less than 10% control levels of growth occurred, as assessed by the measurement of optical density at 600 nm (1 OD_{600} $\approx 3 \times 10^9$ CFU/mL).

Cell-Based Assays. Apoptosis in KB cells was assessed by measuring luminescence due to caspase-3/7 induction, with the Caspase-Glo 3/7 kit (Promega). In this assay, a Z-DEVD proluminescent substrate produces light in the presence of caspase-3/7, ATP, O_2, and Glo luciferase. A 10^{-8} M docetaxel concentration used as internal standard induced caspase activity by a factor of 2. Toxicity assays were performed with the CellTiter 96 AQeous One solution proliferation assay kit (Promega), using colorimetric measurement at 490 nm. All assays were carried out in triplicate with a Biomek workstation (Beckman) in 96-well plates.

3D Modeling. All PDF sequences were numbered as for the EcPDF sequence, as previously described.[16] A substitution of residue X in any PDF indicates that the substitution concerns the residue corresponding to amino acid X in EcPDF. Three-dimensional (3D) modeling was carried out with Insight II software (Accelrys). The 3D structures of *Pseudomonas aeruginosa* PDF (PaPDF1) bound to a benzathiozinone–hydroxamic (BTH) derivative (PDB entry 1S17)[41] and PaPDF1 bound to actinonin (PDB entry 1LRY)[16] were aligned. Compound **6b** was constructed with the Sketcher module, aligned on the structure of both actinonin and BTH, using the hydroxamate group as a fixed anchor and was used to replace either compound in the 3D structure. The **6b** structure docked to PaPDF1 was subjected to further energy minimization with the CharmM force field, and the lowest energy structure was selected.

Supporting Information Available: Additional details for the synthesis of the various PDFI described in Schemes 2 and 3, a table listing the purities of target compounds, Figure S1 showing the results of 3D modeling of the PDF/**6b** complex, and Figures S2 and S3 showing the results from kinetic studies of the interaction between PDF and **6b**. This material is available free of charge via the Internet at http://pubs.acs.org.

References

(1) Hughes, D. Exploiting genomics, genetics and chemistry to combat antibiotic resistance. *Nat. Rev. Genet.* **2003**, *4*, 432−441.

(2) Miesel, L.; Greene, J.; Black, T. A. Genetic strategies for antibacterial drug discovery. *Nat. Rev. Genet.* **2003**, *4*, 442−456.

(3) Mills, S. D. When will the genomics investment pay off for antibacterial discovery? *Biochem. Pharmacol.* **2006**, *71*, 1096−1102.

(4) Boularot, A.; Giglione, C.; Artaud, I.; Meinnel, T. Structure−activity relationship and therapeutic potential of peptide deformylase inhibitors. *Curr. Opin. Invest. Drugs* **2004**, *5*, 809−822.

(5) Jain, R.; Chen, D.; White, R. J.; Patel, D. V.; Yuan, Z. Bacterial peptide deformylase inhibitors: a new class of antibacterial agents. *Curr. Med. Chem.* **2005**, *12*, 1607−1621.

(6) Lee, M. D.; Antczak, C.; Li, Y.; Sirotnak, F. M.; Bornmann, W. G.; Scheinberg, D. A. A new human peptide deformylase inhibitable by actinonin. *Biochem. Biophys. Res. Commun.* **2003**, *312*, 309−315.

(7) Nguyen, K. T.; Hu, X.; Colton, C.; Chakrabarti, R.; Zhu, M. X.; Pei, D. Characterization of a human peptide deformylase: Implications for antibacterial drug design. *Biochemistry* **2003**, *42*, 9952−9958.

(8) Serero, A.; Giglione, C.; Sardini, A.; Martinez Sanz, J.; Meinnel, T. An unusual peptide deformylase features in the human mitochondrial N-terminal methionine excision pathway. *J. Biol. Chem.* **2003**, *278*, 52953−52963.

(9) Giglione, C.; Pierre, M.; Meinnel, T. Peptide deformylase as a target for new generation, broad spectrum antimicrobial agents. *Mol. Microbiol.* **2000**, *36*, 1197−1205.

(10) Yuan, Z.; Trias, J.; White, R. J. Deformylase as a novel antibacterial target. *Drug Discovery Today* **2001**, *6*, 954−961.

(11) Giglione, C.; Boularot, A.; Meinnel, T. Protein N-terminal methionine excision. *Cell. Mol. Life Sci.* **2004**, *61*, 1455−1474.

(12) Lee, M. D.; She, Y.; Soskis, M. J.; Borella, C. P.; Gardner, J. R.; Hayes, P. A.; Dy, B. M.; Heaney, M. L.; Philips, M. R.; Bornmann, W. G.; Sirotnak, F. M.; Scheinberg, D. A. Human mitochondrial peptide deformylase, a new anticancer target of actinonin-based antibiotics. *J. Clin. Invest.* **2004**, *114*, 1107−1116.

(13) Leszczyniecka, M.; Bhatia, U.; Cueto, M.; Nirmala, N. R.; Towbin, H.; Vattay, A.; Wang, B.; Zabludoff, S.; Phillips, P. E. MAP1D, a novel methionine aminopeptidase family member is overexpressed in colon cancer. *Oncogene*, in press.

(14) Xu, Y.; Lai, L. T.; Gabrilove, J. L.; Scheinberg, D. A. Antitumor activity of actinonin *in vitro* and *in vivo*. *Clin. Cancer Res.* **1998**, *4*, 171−176.

(15) Grujic, M.; Renko, M. Aminopeptidase inhibitors bestatin and actinonin inhibit cell proliferation of myeloma cells predominantly by intracellular interactions. *Cancer Lett.* **2002**, *182*, 113−119.

(16) Guilloteau, J. P.; Mathieu, M.; Giglione, C.; Blanc, V.; Dupuy, A.; Chevrier, M.; Gil, P.; Famechon, A.; Meinnel, T.; Mikol, V. The crystal structures of four peptide deformylases bound to the antibiotic actinonin reveal two distinct types: a platform for the structure-based design of antibacterial agents. *J. Mol. Biol.* **2002**, *320*, 951−962.

(17) Ragusa, S.; Mouchet, P.; Lazennec, C.; Dive, V.; Meinnel, T. Substrate recognition and selectivity of peptide deformylase. Similarities and differences with metzincins and thermolysin. *J. Mol. Biol.* **1999**, *289*, 1445−1457.

(18) Fieulaine, S.; Juillan-Binard, C.; Serero, A.; Dardel, F.; Giglione, C.; Meinnel, T.; Ferrer, J. L. The crystal structure of mitochondrial (type 1A) peptide deformylase provides clear guidelines for the design of inhibitors specific for the bacterial forms. *J. Biol. Chem.* **2005**, *280*, 42315−42324.

(19) Serero, A.; Giglione, C.; Meinnel, T. Distinctive features of the two classes of eukaryotic peptide deformylases. *J. Mol. Biol* **2001**, *314*, 695−708.

(20) Meinnel, T.; Blanquet, S.; Dardel, F. A new subclass of the zinc metalloproteases superfamily revealed by the solution structure of peptide deformylase. *J. Mol. Biol.* **1996**, *262*, 375−386.

(21) Meinnel, T.; Patiny, L.; Ragusa, S.; Blanquet, S. Design and synthesis of substrate analogue inhibitors of peptide deformylase. *Biochemistry* **1999**, *38*, 4287−4295.

(22) Mayer, M.; Meyer, B. Group epitope mapping by saturation transfer difference NMR to identify segments of a ligand in direct contact with a protein receptor. *J. Am. Chem. Soc.* **2001**, *123*, 6108−6117.

(23) Van Aller, G. S.; Nandigama, R.; Petit, C. M.; Dewolf, W. E., Jr.; Quinn, C. J.; Aubart, K. M.; Zalacain, M.; Christensen, S. B.; Copeland, R. A.; Lai, Z. Mechanism of time-dependent inhibition of polypeptide deformylase by actinonin. *Biochemistry* **2005**, *44*, 253−260.

(24) Nguyen, K. T.; Hu, X.; Pei, D. Slow-binding inhibition of peptide deformylase by cyclic peptidomimetics as revealed by a new spectrophotometric assay. *Bioorg. Chem.* **2004**, *32*, 178−191.

(25) Morrison, J. F.; Walsh, C. T. The behavior and significance of slow-binding enzyme inhibitors. *Adv. Enzymol. Relat. Areas Mol. Biol.* **1988**, *61*, 201−301.

(26) Henderson, P. J. A linear equation that describes the steady-state kinetics of enzymes and subcellular particles interacting with tightly bound inhibitors. *Biochem. J.* **1972**, *127*, 321−333.

(27) Haas, M.; Beyer, D.; Gahlmann, R.; Freiberg, C. YkrB is the main peptide deformylase in *Bacillus subtilis*, a eubacterium containing two functional peptide deformylases. *Microbiology* **2001**, *147*, 1783−1791.

(28) Giglione, C.; Meinnel, T. Resistance to anti-peptide deformylase drugs. *Expert Opin. Ther. Targets* **2001**, *5*, 415−418.

(29) Nilsson, A. I.; Zorzet, A.; Kanth, A.; Dahlstrom, S.; Berg, O. G.; Andersson, D. I. Reducing the fitness cost of antibiotic resistance by amplification of initiator tRNA genes. *Proc. Natl. Acad. Sci. U.S.A.* **2006**, *103*, 6976−6981.

(30) Clements, J. M.; Beckett, R. P.; Brown, A.; Catlin, G.; Lobell, M.; Palan, S.; Thomas, W.; Whittaker, M.; Wood, S.; Salama, S.; Baker, P. J.; Rodgers, H. F.; Barynin, V.; Rice, D. W.; Hunter, M. G. Antibiotic activity and characterization of BB-3497, a novel peptide deformylase inhibitor. *Antimicrob. Agents Chemother.* **2001**, *45*, 563−570.

(31) Apfel, C.; Banner, D. W.; Bur, D.; Dietz, M.; Hirata, T.; Hubschwerlen, C.; Locher, H.; Page, M. G.; Pirson, W.; Rosse, G.; Specklin, J. L. Hydroxamic acid derivatives as potent peptide deformylase inhibitors and antibacterial agents. *J. Med. Chem.* **2000**, *43*, 2324−2331.

(32) Ragusa, S.; Blanquet, S.; Meinnel, T. Control of peptide deformylase activity by metal cations. *J. Mol. Biol.* **1998**, *280*, 515−523.

(33) Lazennec, C.; Meinnel, T. Formate dehydrogenase-coupled spectro-photometric assay of peptide deformylase. *Anal. Biochem.* **1997**, *244*, 180−182.

(34) Dardel, F.; Ragusa, S.; Lazennec, C.; Blanquet, S.; Meinnel, T. Solution structure of nickel-peptide deformylase. *J. Mol. Biol.* **1998**, *280*, 501−513.

(35) Tisne, C.; Dardel, F. Optimisation of a peptide library for screening specific RNA ligands by flow-injection NMR. *Comb. Chem. High Throughput Screening* **2002**, *5*, 523−529.

(36) Xiang, J.; Christensen, S.; Liao, X. Peptide deformylase inhibitors, Patent WO-02070653. 2002.

(37) Anagnostopoulos, C.; Crawford, I. P. Transformation studies on the linkage of markers in the tryptophan pathway in *Bacillus subtilis*. *Proc. Natl. Acad. Sci. U.S.A.* **1961**, *47*, 378−390.

(38) Miller, H. I.; Friedman, D. I. An *E. coli* gene product required for λ site-specific recombination. *Cell* **1980**, *20*, 711−719.

(39) Hirel, P.-H.; Lévêque, F.; Mellot, P.; Dardel, F.; Panvert, M.; Mechulam, Y.; Fayat, G. Genetic engineering of methionyl-tRNA synthetase: *in vitro* regeneration of an active synthetase by proteolytic cleavage of a methionyl-tRNA synthetase-β-galactosidase chimeric protein. *Biochimie* **1988**, *70*, 773−782.

(40) Singer, M.; Baker, T. A.; Schnitzler, G.; Deischel, S. M.; Goel, M.; Dove, W.; Jaacks, K. J.; Grossman, A. D.; Erickson, J. W.; Gross, C. A. A collection of strains containing genetically linked alternating antibiotic resistance elements for genetic mapping of *Escherichia coli*. *Microbiol. Rev.* **1989**, *53*, 1−24.

(41) Molteni, V.; He, X.; Nabakka, J.; Yang, K.; Kreusch, A.; Gordon, P.; Bursulaya, B.; Warner, I.; Shin, T.; Biorac, T.; Ryder, N. S.; Goldberg, R.; Doughty, J.; He, Y. Identification of novel potent bicyclic peptide deformylase inhibitors. *Bioorg. Med. Chem. Lett.* **2004**, *14*, 1477−1481.